ELSEVIER

Journal of Materials Processing Technology 121 (2002) 157–166

Journal of Materials Processing Technology

www.elsevier.com/locate/jmatprotec

Combustion synthesis and quasi-isostatic densification of powder cermets

E.A. Olevsky[a,*], E.R. Strutt[b], M.A. Meyers[b]

[a]*Department of Mechanical Engineering, San Diego State University, San Diego, CA 92182-1323, USA*
[b]*Department of Mechanical and Aerospace Engineering, University of California, La Jolla, San Diego, CA 92093-0418, USA*

Received 15 March 2001; accepted 29 November 2001

Abstract

Self-propagating High-temperature synthesis (also known as SHS or combustion synthesis) presents a bright potential for the synthesis of compounds with high degree of purity. However, for many reactions, the product is highly porous, and it must either be pulverized for subsequent densification, or densified while it is still hot and ductile. Densification has successfully been applied to a number of ceramic and metal–ceramic systems by (a) a high-speed forging technique, and (b) by a quasi-static pressing technique using a granular pressure-transmitting medium (PTM). The reactive mixture and PTM are placed in a piston and cylinder setup and the system is pressurized by uniaxial compression at a pre-established time after reaction completion. The state-of-stress is close to isostatic and the process is therefore termed as quasi-isostatic pressing (QIP). Modeling of the densification was carried out using the Skorohod constitutive equation; comparison of the results with experimental distortion obtained in indentation experiments enables obtaining equation parameters. The distortion undergone by the combustion synthesis products during QIP densification was modeled using the appropriately verified constitutive equation and assuming a linear elastic response for the granular PTM.

Keywords: Quasi-isostatic pressing; Combustion synthesis; Constitutive modeling; Cermets

1. Introduction

Self-propagating high-temperature synthesis (SHS) is a novel processing technique that has been investigated since the late 1960s [1–4]. SHS is based on the ability of highly exothermic reactions to become self-sustaining and to propagate as a combustion wave. With this technique, a pressed compact with metal and nonmetal powder components is ignited locally at one end. Once ignited, the reaction itself produces sufficient energy to preheat the powder ahead of the wave front to the ignition temperature. When the temperature of this powder reaches the ignition temperature, it also begins to react and generate heat, which is conducted further down the compact. SHS is simply a process of repeated ignition, reaction, and heat conduction.

Although SHS proves to be an energy efficient technique with the capability of producing high purity products, it has not been actively utilized by the manufacturing industry. This is due, in part, to the large amount of porosity in the as synthesized material. During the reaction, gas evolution of volatile impurities leads to lateral escape channels and longitudinal expansion. The concentration of voids can exceed 50%.

2. Densification methods

In order for the benefits of SHS to be realized for the production of structural cermets, the process must be combined with a densification step. Typically researchers have investigated the removal of porosity by the application of a mechanical load while the product is at a high enough temperature to sustain material flow without brittle failure. Examples of techniques include hot-pressing (HIPing), extrusion, and rolling. One of the first densification methods used explosives, because of the high energy available and the short times involved. Niiler et al. [5,6] used explosive consolidation to densify SHS produced TiC and TiB_2. More recently, Grebe [7] carried out an extensive investigation of shock consolidation of TiC. The unreacted powder compact (green compact) was sandwiched between larger steel anvils. The reaction was allowed to initiate and propagate through the entire compact. An explosive charge, placed on top of the steel plate, was initiated at the top by a detonator and an explosive lens. The energy of the explosive products

* Corresponding author. Fax: +1-619-594-3599.
E-mail address: olevsky@kahuna.sdsu.edu (E.A. Olevsky).

0924-0136/02/$ – see front matter
PII: S0924-0136(01)01236-5

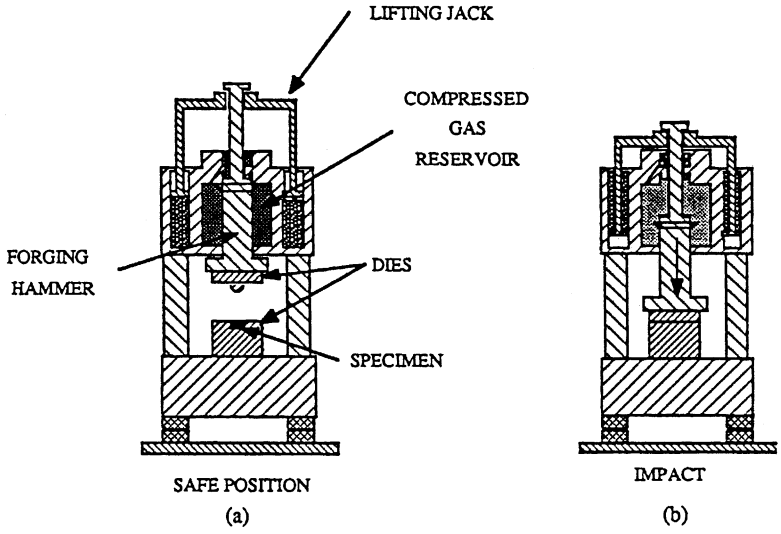

Fig. 1. Experimental setup for the SHS/dynamic compaction (impact forging) technique. (a) Loading position; (b) position at impact.

accelerated the plate down and could, under optimum conditions, lead to the densification (without fragmentation) of the product.

An alternative method was developed by LaSalvia et al. [8–11] and Hoke et al. [12,13]. This is the dynamic compaction or impact forging technique, which resulted in the successful densification of a number of SHS synthesized ceramics and composites. The equipment used is shown in Fig. 1. A gas driven high-speed forging machine (Dynapak) was used. The specimen is placed on a massive steel anvil (pre-heated) and the reaction is ignited. Once the reaction is complete, and at a pre-established time delay, the forging hammer is activated and the die strikes the specimen (Fig. 1(b)). Impact velocities in the 10–15 m/s range were routinely obtained through this method, which allows better control than the explosive consolidation method.

The stress state in explosive and dynamic consolidation is dictated by the loading direction and lateral confinement. Complete isostatic conditions are only obtained in HIPing machines, which are very costly. As a low-cost solution for consolidating porous samples, Gorokhov et al. [14] in the Soviet Union and Lichti and Hofstatter [15] in the United States proposed surrounding the material with granular particulate and then applying a uniaxial load. The procedure is presented in Fig. 2. The particulate acts as a pressure-transmitting medium (PTM) and redistributes the applied axial load to create a stress profile more similar to that of isostatic pressing. This technique is referred to as the Ceracon process [16] or quasi-isostatic pressing (QIP) [17–20].

The simplicity of the QIP process is well-suited for combining it with SHS, into a single synthesis and densification process. This was first done by Raman et al. [21,22]. In the SHS/Ceracon process, the sample is ignited by the pre-heated PTM and densified immediately after passage of the wave front. The granular PTM-thermally insulates the material from the surrounding die wall and allows temperatures to approach the adiabatic condition. Several granular mixtures have been used as a PTM. Among those, alumina, graphite, and alumina–graphite mixtures present the best response for the current application. An important characteristic of the PTM is to provide thermal insulation of the compact, thereby minimizing its cracking. Fig. 3 shows an SEM micrograph of the alumina–graphite mixture. The powder slowly breaks down after successive pressurization cycles, mainly through the fracturing of the alumina particles.

In the current research, the sample is embedded in the PTM prior to initiation of the combustion reaction. The sample is ignited remotely by an electrochemical match [10] via a layer of loose Ti + C powder. The uniaxial load is applied 10–30 s after ignition. This is in contrast to Raman's [21,22] technique, in which hot PTM was poured on the green compact, igniting the combustion.

Optimizing the consolidation process requires predicting the shape and volume changes of a hot porous body subjected

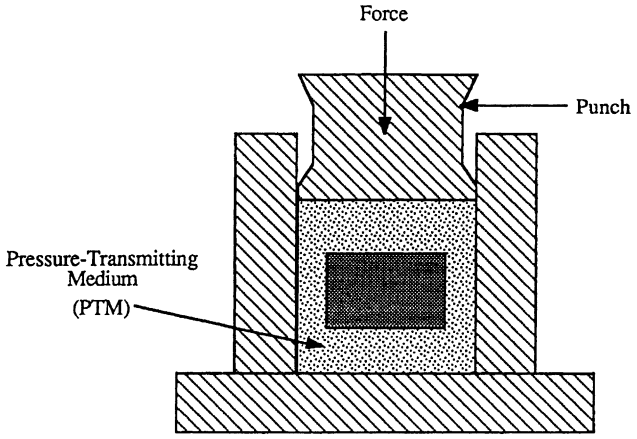

Fig. 2. Experimental setup for the SHS/QIP technique.

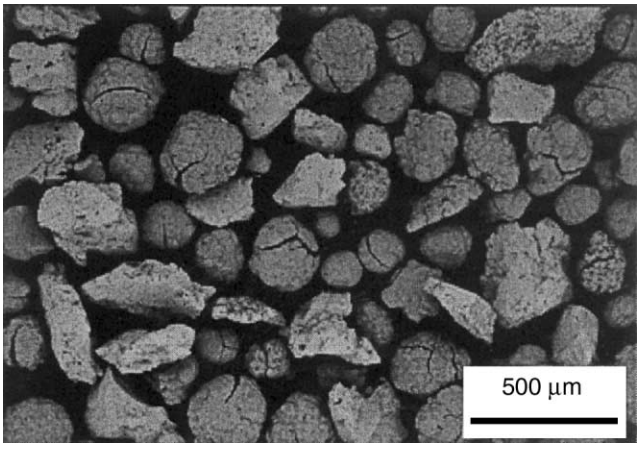

Fig. 3. SEM micrograph of the alumina–graphite PTM. The graphite particles are generally spheroidal in shape with surface fissures; the alumina particles are tabular shaped with closed intergranular pores.

to a mechanical load. Factors that influence the macroscopic deformation during QIP include the porosities of both the PTM and the as-reacted material, as well as their respective constitutive properties. The investigation of the effect of these factors on shape change during QIP is one of the objectives of the present work.

3. Shape change during QIP

3.1. Theory

The objective of this section is to provide a framework for calculating the shape distortion of an initially cylindrical specimen subjected to QIP. The full prediction of distortion requires finite element computation. The calculation of the change in the height (H)/diameter ($2R$) ratio (also called aspect ratio) as a function of the mechanical properties of the PTM and porous sample can be made by analytical methods.

For this analysis, the constitutive behavior of the PTM is assumed to be elastic [15]. The constitutive behavior of the porous body is assumed to be nonlinearly viscous. Nonlinear-viscous mechanical behavior is typical of powdered materials under conditions of hot compaction or two-phase composites containing liquid. It is also assumed that the stresses are uniform within both the PTM and porous body. For simplicity, a cylindrical geometry is assumed, and cylindrical coordinate system is used throughout this paper. The procedure is described below.

3.2. Equations describing the constitutive behavior of a porous specimen

The mechanical response of a nonlinear-viscous porous body can be described [23–26] by a rheological (constitutive) relationship connecting components of stress tensor σ_{ij} and strain rate tensor $\dot{e}_{ij}$

$$\sigma_{ij} = A\left(\frac{\sqrt{\varphi\dot{\gamma}^2 + \psi\dot{e}^2}}{\sqrt{1-\theta}}\right)^{n-1}\left[\varphi\dot{e}_{ij} + \left(\psi - \frac{1}{3}\varphi\right)\dot{e}\delta_{ij}\right] \quad (1)$$

where A and n are material creep parameters; φ and ψ are the shear and bulk normalized viscosity moduli, which depend on porosity θ (e.g., following [23–26], $\varphi = (1-\theta)^2$, $\psi = (2/3)((1-\theta)^3/\theta)$; δ_{ij} is a Kronecker symbol ($\delta_{ij} = 1$ if $i = j$ and $\delta_{ij} = 0$ if $i \neq j$); $\dot{e}$ is the first invariant of the strain rate tensor, i.e., the sum of tensor diagonal components: $\dot{e} = \dot{e}_{11} + \dot{e}_{22} + \dot{e}_{33}$; $\dot{\gamma}$ is the shape change rate. In cylindrical coordinates, the ratio of the radial σ_{rr} and axial σ_{zz} stresses is

$$\frac{\sigma_{rr}}{\sigma_{zz}}(\text{specimen}) = \frac{\varphi\dot{e}_{rr} + (\psi - (1/3)\varphi)\dot{e}}{\varphi\dot{e}_{zz} + (\psi - (1/3)\varphi)\dot{e}} \quad (2)$$

The volume change rate $\dot{e}$ and the shape change rate $\dot{\gamma}$ in cylindrical coordinates are given by

$$\dot{e} = \dot{e}_{zz} + 2\dot{e}_{rr} = \left[1 + 2\left(\frac{\dot{e}_{rr}}{\dot{e}_{zz}}\right)\right]\dot{e}_{zz} = \frac{\dot{\theta}}{1-\theta} \quad (3)$$

$$\dot{\gamma} = \sqrt{\frac{2}{3}}|\dot{e}_{zz} - \dot{e}_{rr}| = \sqrt{\frac{2}{3}}\left|1 - \left(\frac{\dot{e}_{rr}}{\dot{e}_{zz}}\right)\right||\dot{e}_{zz}| \quad (4)$$

where $\dot{e}_{zz}$, $\dot{e}_{rr}$, and θ are the axial strain rate, radial strain rate, and porosity, respectively. For a cylindrical specimen, the axial and radial strain rates are also given by

$$\dot{e}_{zz} = \frac{\dot{H}}{H}, \qquad \dot{e}_{rr} = \frac{\dot{R}}{R} \quad (5)$$

where H and R are the instantaneous cylinder height and radius, respectively. Eq. (4) gives the following relationship for the shape change rate:

$$\dot{\gamma} = \sqrt{\frac{2}{3}}\left|\frac{\dot{H}}{H} - \frac{\dot{R}}{R}\right| \quad (6)$$

This expression will be used to derive relationships between the height and radius of the cylindrical specimen and porosity.

3.3. Equations describing the constitutive behavior of PTM

For the PTM, the radial and axial stresses are related to the axial strain e_{zz} by Hooke's law and are given by

$$\sigma_{rr} = \left[\frac{v}{(1+v)(1-2v)}\right]E\varepsilon_{zz} \quad (7)$$

$$\sigma_{zz} = \left[\frac{1-v}{(1+v)(1-2v)}\right]E\varepsilon_{zz} \quad (8)$$

where v and E are the Poisson's ratio and Young's modulus for the PTM. These depend upon PTM porosity θ_p and are

given by

$$v = \frac{2 - 3\theta_p}{4 - 3\theta_p} \tag{9}$$

$$E = 4E_0\left[\frac{(1-\theta_p)^2}{4-3\theta_p}\right] \tag{10}$$

where E_0 is the Young's modulus of the granular material making up the PTM. The ratio of the radial stress to the axial stress is therefore given by

$$\frac{\sigma_{rr}}{\sigma_{zz}}(\text{PTM}) = \frac{v}{1-v} = \frac{2-3\theta_p}{2} = \frac{1}{k} \tag{11}$$

3.4. Equations describing the constitutive behavior of a porous specimen embedded in PTM

It is assumed that the presence of the porous cylindrical body within the PTM provides a negligible effect on its state-of-stress as a result of the applied axial load. This is equivalent to imagining the porous cylindrical body embedded in an infinitely extended PTM with a far-field applied stress σ_{zz}^{∞} at its boundary. The PTM itself is assumed to be under the condition of uniaxial load with lateral confinement (i.e., pressing in a rigid die). Therefore, the sample can be considered under conditions of biaxial loading.

Since the specimen dimensions are assumed to be small compared to the PTM, the ratio of the radial stress to the axial stress in the specimen $((\sigma_{rr}/\sigma_{zz})(\text{specimen}))$ is assumed to be equal to the ratio of the radial stress to the axial stress in the PTM $((\sigma_{rr}/\sigma_{zz})(\text{PTM}))$. Setting Eq. (2) equal to Eq. (11) yields the following equation for the radial/axial strain rate ratio:

$$\frac{\dot{e}_{rr}}{\dot{e}_{zz}} = \frac{k(2-3\theta)-2}{2(2-3\theta)-k(4-3\theta)} \tag{12}$$

If $k = 2/(2-3\theta)$ (which means that $\theta = \theta_p$), then $\dot{e}_{rr} = 0$, and we have the conditions of pressing in a rigid die. If $k = 1$ (i.e., if $\theta_p = 0$ which means that PTM is an incompressible material), $\dot{e}_{rr} = \dot{e}_{zz}$, and we have the conditions of isostatic pressing. If $k \to \infty$ (i.e., if $\theta_p = 2/3$) which approximately corresponds to the density of packed isomeric spherical particles then $\dot{e}_{rr} = ((3\theta-2)/(4-3\theta))\dot{e}_{zz}$, and we have the conditions of free up-setting.

Combining Eqs. (3), (5) and (12) gives the following expression for the axial strain rate in terms of the rate-of-change of porosity:

$$\dot{e}_{zz} = \frac{\dot{H}}{H} = \frac{1}{3}\left[\frac{2\theta_p + (1-3\theta_p)\theta}{(1-\theta_p)(1-\theta)}\right]\frac{\dot{\theta}}{\theta} \tag{13}$$

Combining Eqs. (3), (12) and (13) gives the following expression for the radial strain rate in terms of the rate-of-change of porosity:

$$\dot{e}_{rr} = \frac{\dot{R}}{R} = \frac{1}{3}\left[\frac{\theta-\theta_p}{(1-\theta_p)(1-\theta)}\right]\frac{\dot{\theta}}{\theta} \tag{14}$$

The shape change rate can be represented as follows:

$$\dot{\gamma} = 2\sqrt{6}\left|\frac{(1-\theta)(1-k)}{2(2-3\theta)-k(4-3\theta)}\right||\dot{e}_{zz}| \tag{15}$$

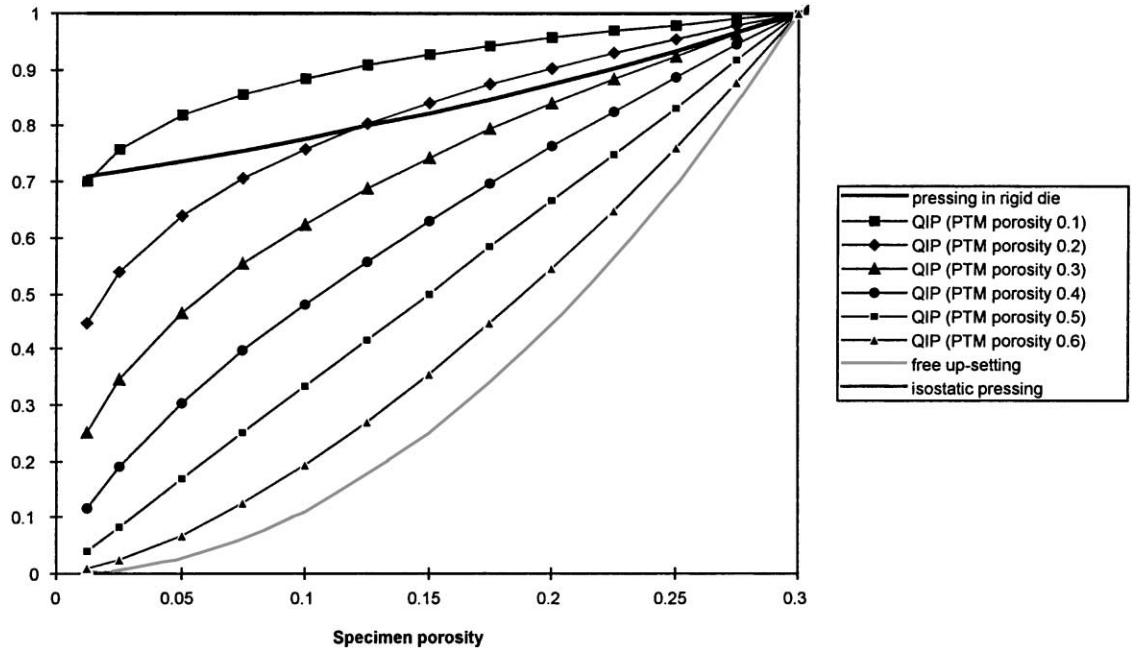

Fig. 4. Shrinkage anisotropy as a function of specimen porosity under QIP.

Subtracting Eq. (14) from (13), and integrating gives the following expression for the aspect ratio H/R:

$$\frac{\dot{H}}{H}-\frac{\dot{R}}{R}=\left(\frac{\theta_p}{1-\theta_p}\right)\frac{\dot{\theta}}{\theta}\Rightarrow\int_{H_0/R_0}^{H/R}\mathrm{d}\ln\left(\frac{H}{R}\right)$$
$$=\left(\frac{\theta_p}{1-\theta_p}\right)\int_{\theta_0}^{\theta}\mathrm{d}\ln\theta\Rightarrow\frac{H}{R}$$
$$=\frac{H_0}{R_0}\left(\frac{\theta}{\theta_0}\right)^{\theta_p/(1-\theta_p)} \tag{16}$$

In deriving Eq. (16), it was assumed that θ_p is constant. Eq. (16) indicates that the change in the aspect ratio H/R does not depend upon the constitutive behavior of either the PTM or densified body, but depends only on the PTM's porosity and the body's initial density and dimensional parameters.

In Fig. 4, the curves are shown corresponding, for various PTM porosities, to the relationships between the change of the aspect ratio expressed by the relationship $(H/R)/(H_0/R_0)$ and sample's porosity. For comparison, the curves corresponding to the conditions of free up-setting, pressing in a rigid die ($\dot{e}_{rr}/\dot{e}_{zz}=0$) and isostatic pressing ($\dot{e}_{rr}/\dot{e}_{zz}=1$) are shown too [27].

The initial porosity of the sample is assumed to be $\theta_0=0.3$.

The calculation results indicate that, for sufficiently dense PTM, having porosity $\theta_p<0.2$, the deformation state under QIP is close to the isostatic one. However, for most cases, in the capacity of PTM, industrial sand (alumina) or graphite powder in a loose state are used. Therefore usually $\theta_p>0.2$. This means that the aspect ratio evolution under QIP can be close to that one obtained under the conditions of pressing in a rigid die or free up-setting.

4. Indentation experiments and constitutive response

As mentioned above, the complete description of the densification process requires knowledge of the constitutive response of the material. It is important to obtain this constitutive description, for implementation into computational codes, which can then predict the response of the material under a variety of loading configurations and enable a predictive shape capability. The parameters in Eq. (1) can be experimentally measured by performing indentation tests. Fig. 5(a) shows the experimental setup used. A disk-shaped green compact was placed in a uniaxial testing machine (Instron) and ignited. After the reaction was completed, a cylindrical indenter was moved onto the specimen at a prescribed velocity, producing an indentation, whose cross-section is shown in Fig. 5(b). The velocity of the sintered SiC indenter was 0.4 m/s. Fig. 6(a) shows the experimental stress–strain curve for combustion synthesized TiC–NiTi. The stress is very low (below 10 MPa) up to a strain of 0.6 (compressive), and then rises sharply.

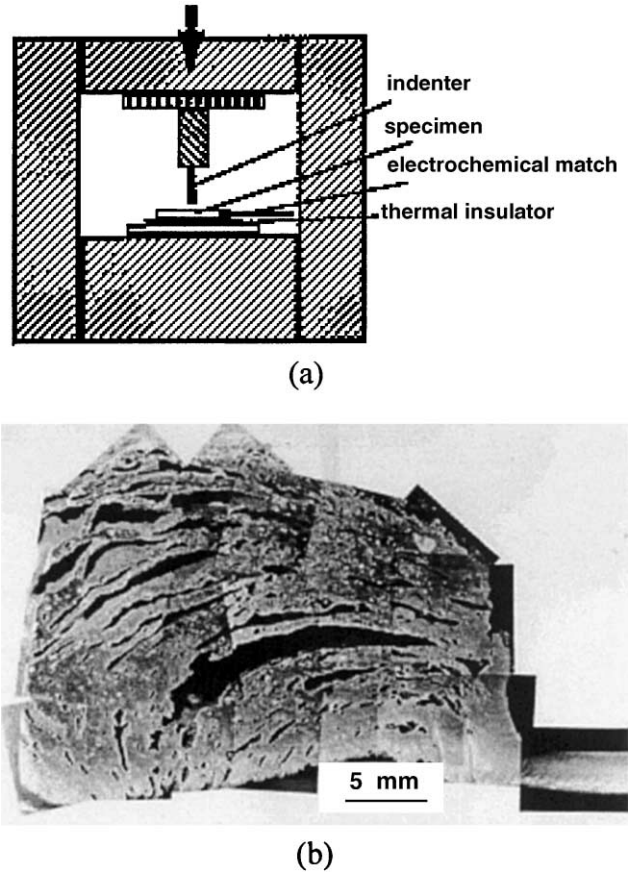

Fig. 5. (a) Schematic of indentation setup; (b) cross-section of indented TiC–NiTi specimen, showing distortion and full densification under indenter.

In order to obtain an analytical solution of the indentation process, the uniaxial up-setting of a porous cylinder with a radius smaller than the indenter is modeled. Friction is neglected, as well as the distortion of the compact outside of the main deformation zone.

During free upsetting, the applied stresses on the lateral surfaces are equal to zero. By setting $\sigma_{rr}=0$ in Eq. (1), one can obtain the following relationship between the axial and radial strain rates:

$$\frac{\dot{e}_{rr}}{\dot{e}_{zz}}=\frac{1-3(\psi/\varphi)}{1+6(\psi/\varphi)}=-\left(\frac{2-3\theta}{4-3\theta}\right) \tag{17}$$

Combining Eqs. (1), (3), (4) and (17) and considering that $\sigma_{zz}<0$, the following expression for the axial stress is obtained:

$$\sigma_{zz}=-A(6)^{(n+1)/2}\left[\frac{(1-\theta)^{n+2}}{(4-3\theta)^{(n+1)/2}}\right]|\dot{e}_{zz}|^n \tag{18}$$

The latter equation can be transformed as follows:

$$\frac{|\sigma_z|}{A}\left(\frac{H_0}{V_p}\right)^n=6^{(n+1)/2}\left[\frac{(1-\theta)^{n+2}}{(4-3\theta)^{(n+1)/2}}\right]\left(\frac{H_0}{H}\right)^n \tag{19}$$

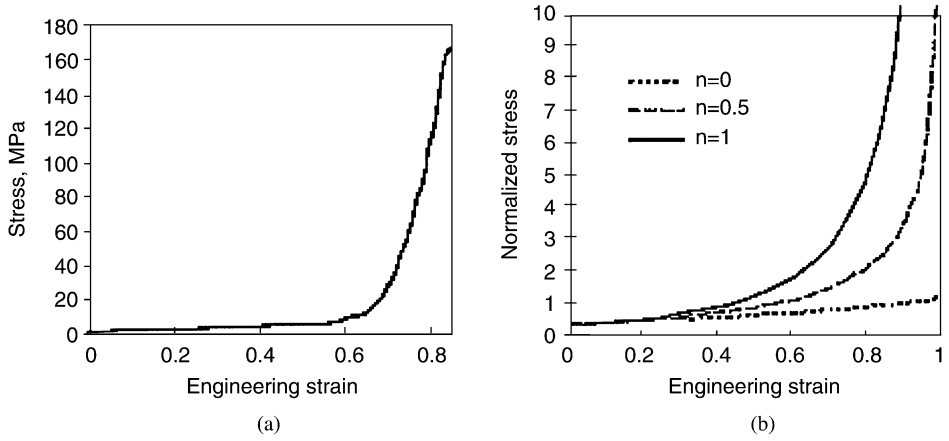

(a) (b)

Fig. 6. (a) Experimentally obtained stress strain response of SHS product (TiC–NiTi); (b) predictions of stress strain response using Skorohod equation and analytical framework for free-upsetting geometry ($\sigma_{rr} = 0$), for different values of rheology parameter n ($A = 180$ MPA s^n).

where H_0 is the initial height of the porous cylinder and V_p the constant velocity of the indenter. From Eqs. (3), (5) and (17) it follows that:

$$\frac{\theta}{1-\theta} = \frac{3\theta}{4-3\theta}\frac{\dot{H}}{H} \tag{20}$$

Integration of Eq. (20) gives

$$\left(\frac{\theta}{\theta_0}\right)^4 \frac{1-\theta_0}{1-\theta} = \left(\frac{H}{H_0}\right)^3 \tag{21}$$

where θ_0 is the initial porosity before the indentation.

The solution of Eqs. (19) and (21) enables the determination of the stress–strain dependence characterizing the mechanical response of the porous material.

The dependence of the normalized stress $(|\sigma_z|/A)(H_0/V_p)^n$ on the engineering strain is shown in Fig. 6(b) for different values of the strain rate sensitivity n. The engineering strain is calculated as $(H_0 - H)/H$. Here it should be noted that the dimensionless stress depends on the strain rate sensitivity n itself.

Using Eqs. (19) and (21), one can find the constitutive properties (coefficients A and n) which provide the best fit for the experimental data given in Fig. 6(a). It is determined that the following values: $A = 180$ MPa $s^{0.2}$, $n = 0.2$ provide the best fit to the experimental data.

5. Characterization of material

A number of ceramics and cermets were produced by our group using the methods described herein: TiC [8,9], TiB_2 [12,13], TiC–Ni [10], TiC–Ni–Mo [11], TiB_2–Al_2O [28], TiC–NiTi [18–20], TiB_2–NiTi, TiB_2–SiC [28,29]. Each material requires a specific optimization process to determine the chemistry of the initial powder mixture, the time delay before load application, and the maximum pressure required for complete densification.

Fig. 7 shows the effectiveness of the QIP densification sequence for removing porosity in SHS products. The large voids and lateral channels created during the SHS process are shown in Fig. 7(a) for a TiC–40 vol.% NiTi composite. In Fig. 7(b), these voids have been collapsed by applying a 106 MPa uniaxial pressure after a delay time of 10 s.

One of the principal advantages of SHS is the high purity of the product. The impurities are expelled as gases during the combustion reaction. As a result of this, interfaces and grain boundaries in SHS produced material have a low level of contamination. This is especially advantageous in composites and cermets where interfaces need to have a high cohesive strength. Conventional processing methods produce interfaces with a high level of impurities. The impurities present in the starting powder remain in the product and outline the original powder surfaces. This potentially weakens the interfaces between different grains and/or phases.

Fig. 8 shows TiC produced by SHS/dynamic compaction. The grains are equiaxed and transmission electron microscopy (not shown here; see [8,9]) revealed clean grain boundaries. The grain boundaries are devoid of major inclusions. TiC tiles with dimensions as large as 15 cm × 15 cm × 2.5 cm were produced by the Ceracon process [22]. The mechanical properties are comparable to hot-pressed TiC.

More complex ceramics can also be produced; as an illustration a TiB_2 with the addition of 20% particulate SiC is shown in Fig. 9 [28]. The darker phase is SiC and the lighter phase is TiB_2. The SiC and TiB_2 react to form a eutectic structure shown in the middle of the micrograph. Good cohesion between the two phases was obtained as a result of complete wetting.

The addition of a metallic phase provides additional enhancement in toughness. Several ceramic–metal (cermet) mixtures were successfully synthesized and densified. Fig. 10 shows a TiC–25% Ni cermet. The TiC particles are spheroidal with a size of approximately of 15 μm. The size of the ceramic phase is dependent on the cooling rate. The particle size increases with increasing compact size,

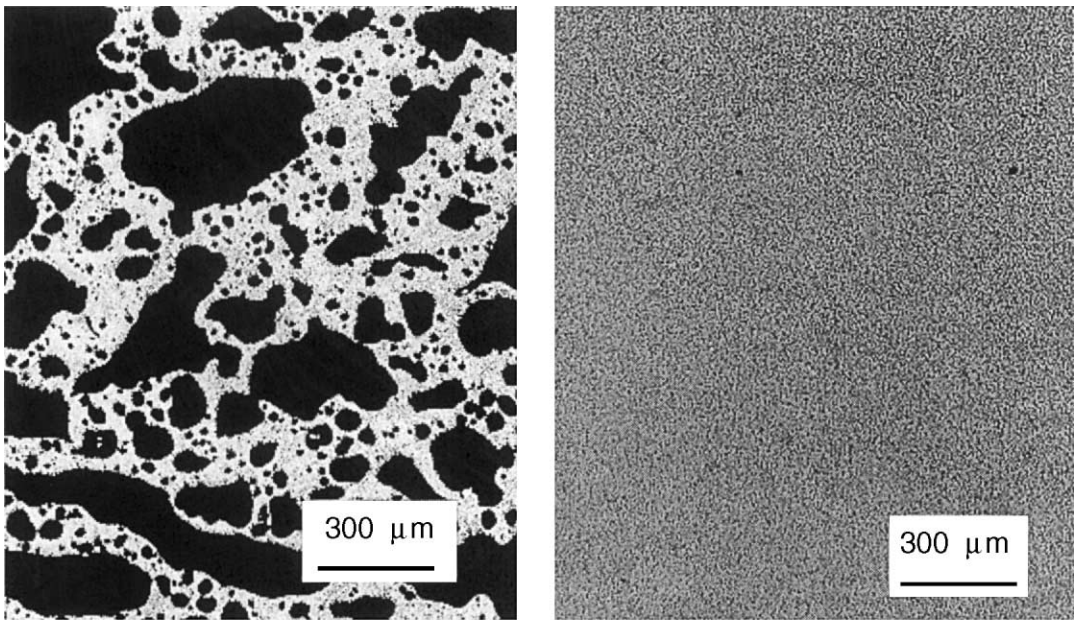

Fig. 7. Comparison of pore structure in SHS synthesized TiC cermet. (a) As-reacted material not subject to post reaction densification; reacted and (b) densified material.

because of the lower cooling rate. It also decreases with increasing Ni additions, because of the lower reaction temperature. The TiC particles grow by a process of Ostwald ripening whereby the large particles grow at the expense of the smaller particles. This is a diffusion controlled mechanism requiring the dissolution of smaller particles into the metallic binder and the reprecipitation of material on the surface of the larger particles. Consequently, processing and microstructural control are closely linked.

Composites using a NiTi matrix show particular promise for hard and tough applications, such as cutting tools [30]. Near stoichiometric NiTi undergoes a martensitic transformation between a cubic phase, B2, and a monoclinic phase, B19′. This transformation, which is responsible for the shape memory and superelastic effects, can be induced by both external and internal stresses. In NiTi, elastic strains between 0.04 (compression) and 0.08 (tension) are produced by the B2 → B19′ transformation. In contrast, the maximum elastic strain that a ceramic phase can accommodate without failure is no more than 0.01. NiTi should increase the resilience of ceramic composites by accommodating strain through the B2 → B19′ transformation, thereby retarding crack initiation.

Two such cermets were synthesized and densified: TiB_2–NiTi and TiC–NiTi. Fig. 11(a) shows a TiB_2–50% NiTi cermet. The grains are faceted and form polyhedra, in

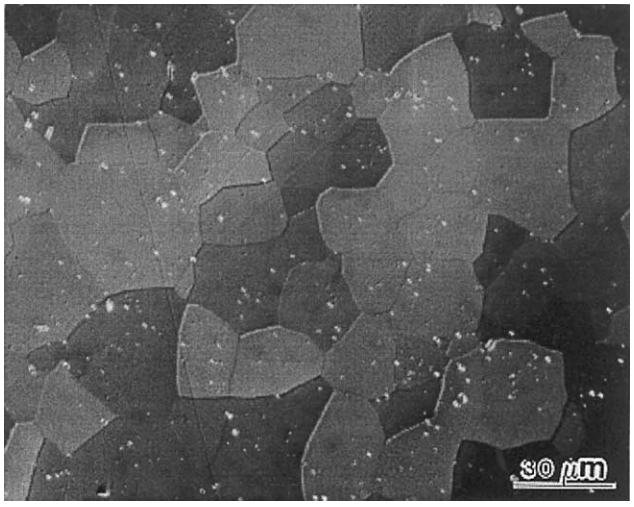

Fig. 8. Optical micrograph of TiC produced by SHS/dynamic compaction.

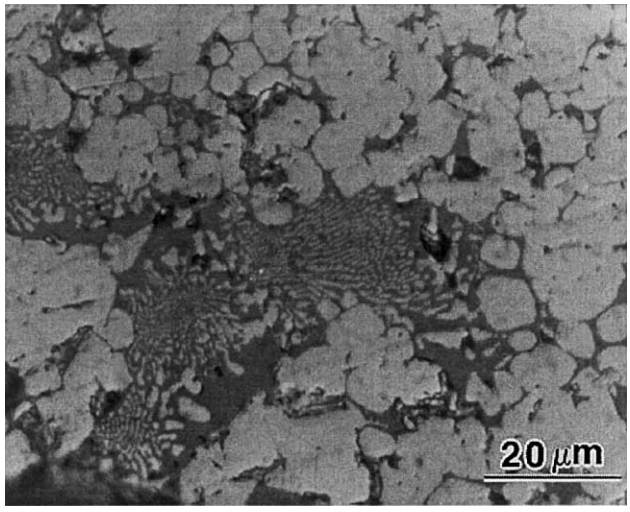

Fig. 9. Microstructure of TiB_2–SiC produced by SHS/dynamic compaction.

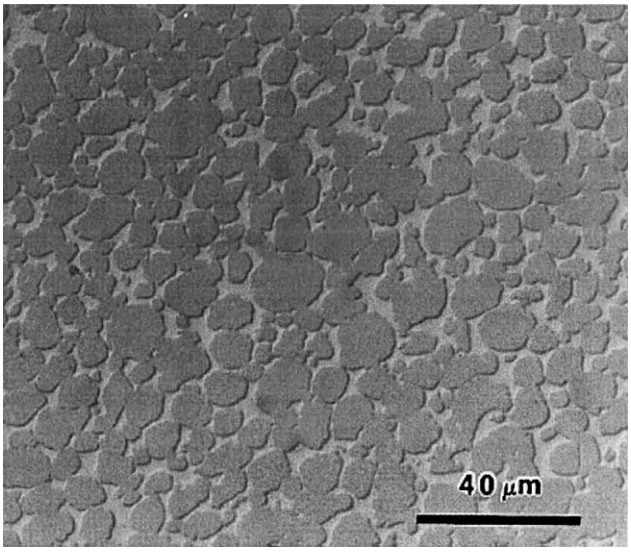

Fig. 10. Microstructure of TiC–25% Ni cermet produced by SHS/dynamic compaction.

contrast with TiC (shown in Fig. 11(b)) where the grains are spherical. There is no visible evidence of contamination in composites produced by SHS. Fig. 12 shows transmission electron micrographs of an SHS produced $TiC_{0.7}$–40 vol.% NiTi composite. The interfaces between the ceramic reinforcement and the matrix are not outlined by impurities. The high reaction temperatures achieved during the SHS effectively drive off all volatile impurities, so that the purity of the product is not limited by the purity of the reactants. Selected area diffraction on the matrix of a $TiC_{0.7}$–40 vol.% NiTi composite, shown in Fig. 13, reveals that the structure of the matrix, at ambient temperature, is cubic B2 NiTi. The diffraction pattern has 6-fold rotational

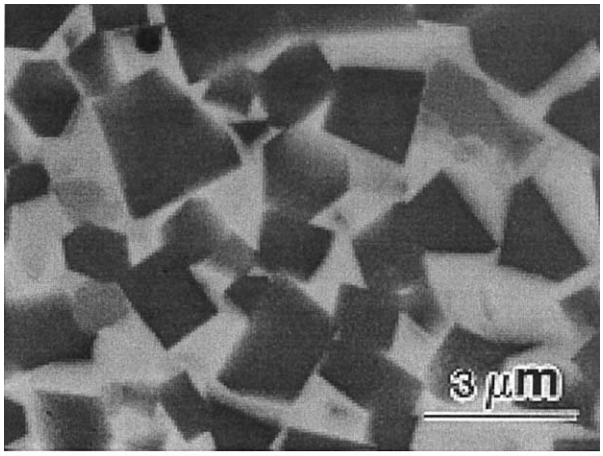

(a)

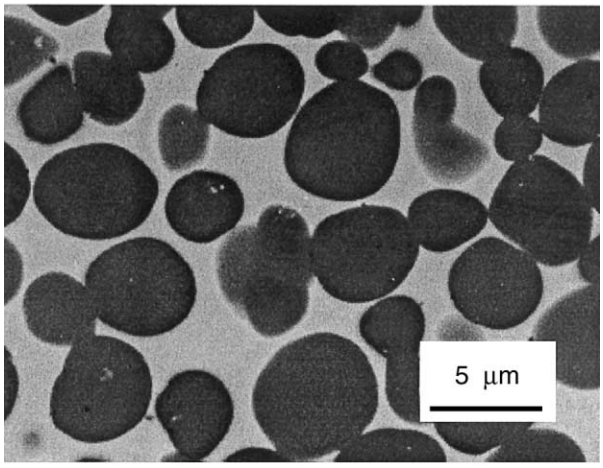

(b)

Fig. 11. Backscattered electron micrographs of (a) TiB_2–50% NiTi and (b) nonstoichiometric $TiC_{0.7}$–40 vol.% NiTi.

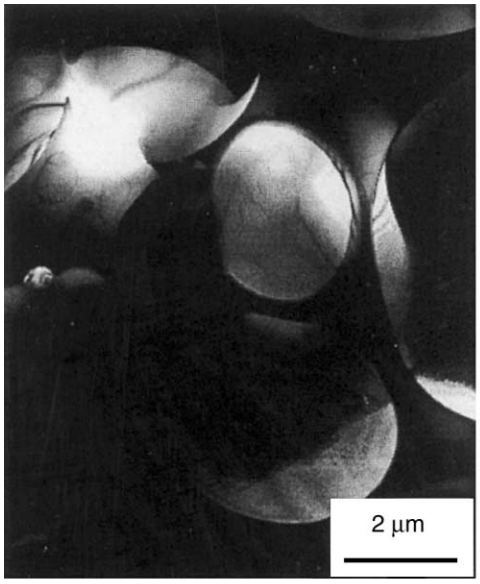

(a)

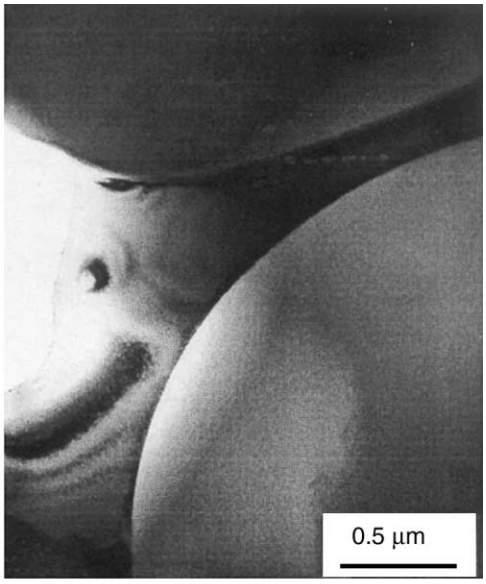

(b)

Fig. 12. Transmission electron micrographs of $TiC_{0.7}$–40 vol.% NiTi showing the interface between the TiC particles and the NiTi matrix.

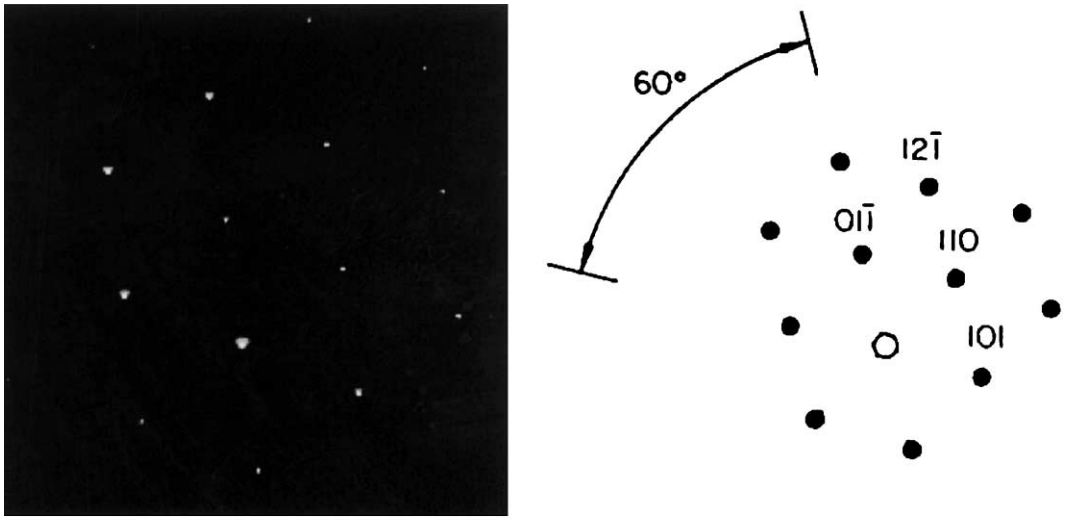

Fig. 13. (a) Selected area diffraction pattern of the matrix of $TiC_{0.7}$–40 vol.% NiTi composite, showing 6-fold rotational symmetry. (b) Predicted diffraction pattern for cubic B2 NiTi along the $[\bar{1}\,1\,1]$ zone axis.

symmetry which excludes the monoclinic structure of the B19′ martensite. The lattice parameter is calculated to be 3.05 Å, which is within 2% of the value reported by JCPDS for B2 NiTi.

6. Conclusions

A brief overview of the principal consolidation methods for SHS products is presented; explosive, dynamic, and quasi-static compaction are described. The use of a granular PTM for the establishment of a state-of-stress that resembles isostatic compression is described. A mathematical model of the QIP is developed, which predicts an essential shape change for large porosities of the PTM. The experimental procedure to obtain the constitutive response of the SHS porous product is described. It consists of a uniaxial indentation test, from which a stress–strain curve is obtained. This curve is then compared with predictions using the Skorohod constitutive equation for porous materials; the basic parameters from the Skorohod equation are obtained from the best fit with experimental results. Microstructures produced by SHS-densification are illustrated, for ceramics (TiC and TiB_2–SiC) and cermets (TiC–Ni, TiB_2–NiTi, and TiC–NiTi).

Acknowledgements

This research is supported by the Army Research Office under the MURI program (Contract DAAH 04-96-1-0376). Discussions with and contributions by Dr. J.C. La Salvia are greatly appreciated. The help of Mr. J.-L. Lemee, Prof. D.K. Kim, Prof. L.W. Meyer, D.A. Hoke and Dr. A. Niiler are gratefully acknowledged. The transmission electron microscopy was kindly carried out by Dr. A.J. Strutt.

References

[1] A.G. Merzhanov, in: Z.A. Munir, J.B. Holt (Eds.), Combustion and Plasma Synthesis of High Temperature Materials, VCH Publishers, New York, 1990, p. 1.
[2] Z.A. Munir, U. Anselmi-Tambourini, Mater. Sci. Res. 3 (1989) 277.
[3] H.C. Yi, J.J. Moore, J. Mater. Sci. 25 (1990) 1159.
[4] J.J. Moore, H.J. Feng, Progr. Mater. Sci. 39 (1995) 243.
[5] A. Niiler, L.J. Kecskes, T. Kottke, P. Netherwood Jr., R.F. Benck, Report BRL-TR-2951, Ballistics Research Laboratory, Aberdeen Proving Ground, MD, 1988.
[6] A. Niiler, T. Kottke, L.J. Kecskes, in: M.A. Meyers, N.N. Thadhani (Eds.), Shock Consolidation of the Combustion Synthesized Ceramics, CETR, Socorro, New Mexico, 1988, p. 101.
[7] H.A. Grebe, High-rate chemical reaction and dynamic high-pressure processing of titanium carbide ceramics, Ph.D. Thesis, New Mexico Institute of Mining and Technology, 1996.
[8] J.C. LaSalvia, M.A. Meyers, Int. J. SHS 4 (1) (1995) 43.
[9] J.C. LaSalvia, L.W. Meyer, M.A. Meyers, J. Am. Ceram. Soc. 75 (3) (1992) 592.
[10] J.C. LaSalvia, M.A. Meyers, D.K. Kim, J. Mater. Synth. Process. 2 (4) (1994) 255.
[11] J.C. LaSalvia, D.K. Kim, M.A. Meyers, Mater. Sci. Eng. A 206 (1996) 71.
[12] D.A. Hoke, M.A. Meyers, L.W. Meyer, G.T. Gray III, Metall. Trans. A 23 (1992) 77.
[13] D.A. Hoke, M.A. Meyers, J. Am. Ceram. Soc. 78 (2) (1994) 275.
[14] V.M. Gorokhov, M.S. Koval'chenko, O.V. Roman, Sov. Powd. Metall. Met. Ceram. 22 (7) (1983) 708.
[15] W.P. Lichti, A.F. Hofstatter, US Patent No. 4 539 175 (3 September 1985).
[16] B.L. Ferguson, A. Kuhn, O.D. Smith, A. Hofstatter, in: K.M. Kulkarni (Ed.), Powder Metallurgy for Full Density Products, New Perspectives in Powder Metallurgy, Vol. 8, Metal Powder Industries Federation, Princeton, NJ, 1987, p. 225.

[17] E.A. Olevsky, J.C. LaSalvia, M.A. Meyers, Adv. Powd. Metall. Particul. Mater. (1997) 20.13–20.19.
[18] E. Olevsky, E. Kristofetz, C. Uzoigwe, M. Meyers, Adv. Powd. Metall. Particul. Mater. (1997) 3.43–3.49.
[19] E.A. Olevsky, E.R. Strutt, M.A. Meyers, Adv. Powd. Metall. Particul. Mater. (1998) 3.93–3.100.
[20] E.A. Olevsky, E.R. Kristofetz, M.A. Meyers, Int. J. Self-propagation High Temp. Synth. 7 (4) (1999) 517–528.
[21] R.V. Raman, S.V. Rele, M.J. Paskowitz, J. Met. (1993) 54.
[22] R.V. Raman, S.V. Rele, S. Poland, J. LaSalvia, M.A. Meyers, A.R. Niiler, J. Met. N 3 (1995) 23.
[23] V. Skorohod, E. Olevsky, M. Shtern, Powd. Metall. Met. Ceram. N 1 (361) (1993) 22.
[24] V. Skorohod, E. Olevsky, M. Shtern, Powd. Metall. Met. Ceram. N 2 (362) (1993) 16.
[25] E. Olevsky, H.J. Dudek, W.A. Kaysser, Acta Met. Mater. 44 (2) (1996) 707.
[26] E.A. Olevsky, Mater. Sci. Eng. Rev. 23 (1998) 41–100.
[27] E.A. Olevsky, J.C. LaSalvia, M.A. Meyers, Densification of porous bodies in a granular pressure-transmitting medium, Part I. Shrinkage anisotropy, in preparation.
[28] M.A. Meyers, J.C. LaSalvia, D.A. Hoke, J.-M. Jamet, D.K. Kim, in: Proceedings of the International Conference on Advanced Synthesis of Engineered Structural Materials, ASM International, Materials Park, OH, 1993, p. 43.
[29] D.A. Hoke, D.K. Kim, J.C. LaSalvia, M.A. Meyers, J. Am. Ceram. Soc. 79 (1996) 177.
[30] D. Goldstein, S.M. Hoover, US Patent No. 5 145 506 (8 September 1992).